



ELSEVIER

Contents lists available at SciVerse ScienceDirect

# Nuclear Instruments and Methods in Physics Research A

journal homepage: [www.elsevier.com/locate/nima](http://www.elsevier.com/locate/nima)

## Algorithms for pulse shape analysis using silicon detectors

S.N. Liddick<sup>a,b,\*</sup>, I.G. Darby<sup>a,c</sup>, R.K. Grzywacz<sup>a,d</sup><sup>a</sup> Department of Physics and Astronomy, University of Tennessee, Knoxville, TN 37919, USA<sup>b</sup> Department of Chemistry and National Superconducting Cyclotron Laboratory, Michigan State University, East Lansing, MI 48824, USA<sup>c</sup> IAEA Nuclear Spectrometry and Applications Laboratory, Physics Section, A-2444, Siebersdorf, Austria<sup>d</sup> Physics Division, Oak Ridge National Laboratory, Oak Ridge, TN 37831, USA

### ARTICLE INFO

#### Article history:

Received 21 September 2011

Received in revised form

29 November 2011

Accepted 10 December 2011

Available online 17 December 2011

#### Keywords:

Digital electronics

Silicon detectors

Decay spectroscopy

### ABSTRACT

The development of digital electronics and their application to nuclear spectroscopy has provided an opportunity to perform experiments beyond the technical capabilities of analog systems. The pulse-shape analysis of Si detectors is described here for the selective identification of pile-up pulses resulting from the sequential alpha decay of  $^{109}\text{Xe}$  and  $^{105}\text{Te}$  isotopes. A two stage offline pulse shape analysis algorithm is described which is able to detect pile-up pulses from the two alpha decays with time differences between the two individual pulses as low as 100 ns over a wide range of relative amplitudes.

© 2011 Elsevier B.V. All rights reserved.

### 1. Introduction

The development of digital pulse processing, wherein the traditional shaping and timing circuitry are replaced by mathematical routines operating on a digitized preamplifier signal have enabled the implementation of sophisticated pulse shape analysis (PSA) algorithms. This allows substantially more information to be extracted from an experimental pulse than is possible with a traditional analog system. Significant effort has been devoted to pursuing digital pulse-shape processing in a variety of applications including; double beta-decay searches [1,2], large HPG tracking arrays [3,4], small animal medical devices [5], room-temperature moderate resolution gamma-ray spectroscopy (CZT) [6], precision timing measurements [7,8], and  $n$ -gamma discrimination [9]. Within silicon detectors, advanced pulse-shape analysis routines have focused on spectroscopic measurement of short-lived proton emission in decay spectroscopy investigations [10] and isotopic identification in reaction measurements [11].

In this paper we discuss another aspect of implementing PSA with silicon detectors, recovering spectroscopic energy and time information from pulses due to the successive alpha decays of  $^{109}\text{Xe}$  and  $^{105}\text{Te}$  which occur within the same physical region of the detector. The experimental data and its interpretation using the methods described in this paper have been previously presented [12–14]. Several factors of the current algorithm are

noteworthy. Both the signal from the implanted ion and subsequent decay come from the same detector and through the same electronics chain. This requires a large dynamic energy range with the limiting case being the discrimination of a low-energy recoil event from a high-energy or summed-energy decay event. Additionally, the distribution of times between the two decay radiations is described by the characteristic decay curve of  $^{105}\text{Te}$  ( $t_{1/2} = 620(70)$  ns [12]) requiring an algorithm that can be used to detect small time differences between the two alpha decay pulses with high efficiency.

Utilization of PSA for decay spectroscopy was first applied to microsecond proton emitters [15] and resulted in the detection of fine structure in the proton decay of  $^{145}\text{Tm}$  [16] and the observation of proton activity from  $^{144}\text{Tm}$  [17]. In this study PSA was employed to identify and characterize those pulses in which a large energy signal from the implantation of a heavy ion into a Si detector was followed by a low energy proton signal within 10  $\mu\text{s}$  ( $^{145}\text{Tm}$ ) or 32  $\mu\text{s}$  ( $^{144}\text{Tm}$ ). This method overcomes the well known phenomena wherein the decay signal following the recoil implant occurs in the overload recovery period of the amplifier [18–20].

An extension of these early techniques enabled the search for the pile-up pulses resulting from the sequential alpha decay of  $^{109}\text{Xe}$  and  $^{105}\text{Te}$ . Due to the short time between the  $^{109}\text{Xe}$  and  $^{105}\text{Te}$  alpha decays ( $^{109}\text{Xe}$   $t_{1/2} = 620$  ns [12]) it was risky to implement the same online triggering scheme used in Refs. [16,17] for selecting pile-up pulses. Instead all traces below a certain energy were recorded [10]. The dramatic increase in the amount of collected data necessitated the development of a selective offline PSA algorithm that could differentiate between the pile-up pulse from the decay of  $^{109}\text{Xe}$  followed by  $^{105}\text{Te}$  and a

\* Corresponding author at: Department of Chemistry and National Superconducting Cyclotron Laboratory, Michigan State University, East Lansing, MI 48824, USA. Tel.: +1 517 908 7690.

E-mail address: [liddick@nsc.lmsu.edu](mailto:liddick@nsc.lmsu.edu) (S.N. Liddick).

normal pulse, the results of which have been reported in Refs. [10,12–14].

The organization of the paper is as follows: in Section 2 the salient details of the experimental setup are provided; in Section 3 the construction of a model pulse shape is described; in Section 4 the breakdown of the PSA into two separate stages is described; in Section 5 the three methods used for the selective identification of pile-up pulses in a thin ( $\sim 65 \mu\text{m}$ ) Si detector resulting from the alpha decays of  $^{109}\text{Xe}$  and  $^{104}\text{Te}$  in rapid succession are described; in Section 6 the characterization of the pile-up pulses in stage 2 is described and finally the results are summarized in Section 7 with an outlook towards future measurements.

## 2. Experimental description

Ions of  $^{109}\text{Xe}$  were produced via heavy ion fusion-evaporation reactions  $^{54}\text{Fe}(^{58}\text{Ni},3n)^{109}\text{Xe}$ , (or the inverse reaction). Mass-109 ions were separated from other reaction products based on  $A/Q$  by the Recoil Mass Spectrometer (RMS) [21], and implanted into a Double-sided Silicon Strip Detector (DSSD). The detector was segmented into 40 strips on both the front and back providing a total of 1600 effective pixels. The decay energy spectrum obtained during the experiment is shown in Fig. 1 and is dominated by the alpha decays of  $^{109}\text{Te}$  (3.107 MeV) and  $^{108}\text{Te}$  (3.318 MeV). The alpha decays from  $^{109}\text{Xe}$  and its daughter,  $^{105}\text{Te}$ , were also detected in the DSSD. The DSSD was read out using DGF4C modules [22]. The incoming preamplifier signal was sampled at 40 MSPS and digitized with a 12-bit ADC. If the energy of the event as determined by an on-board trapezoidal filter was below 9.2 MeV, an experimental trace was recorded for further offline analysis. Each recorded experimental trace was a total of 25  $\mu\text{s}$  long sampled every 25 ns starting 1  $\mu\text{s}$  before the leading edge of the pulse. The first 1  $\mu\text{s}$  of each trace was used to determine a baseline from which the energy of the pulse was measured. The various signal types recorded during a typical experimental run could be separated into five categories and are shown in Fig. 2. The overwhelming majority of the traces were similar to the trace shown in Fig. 2a.

## 3. Ideal response

Differentiating the various experimental signals presented in Fig. 2 on the basis of their unique pulse shapes requires characterizing the response of each detector element and preamplifier chain to alpha radiation to derive the ideal pulse shape, or superpulse (used hereafter). The early implementation of the superpulse technique presented here was previously applied in Ref. [17]. Since each DSSD strip had a separate preamplifier a superpulse was constructed strip-by-strip based on the response to the 5.485 MeV alpha emitted by an open  $^{241}\text{Am}$  source. For

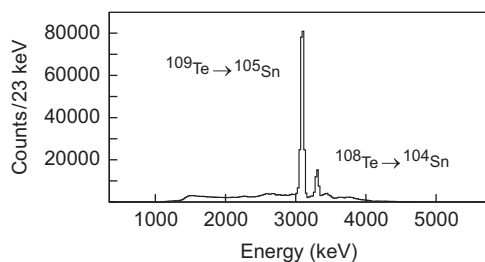


**Fig. 1.** Decay energy spectrum correlated with mass 109 ions from 0 to 9 MeV. The alpha decays of  $^{109}\text{Te}$  and  $^{108}\text{Te}$  are indicated in the figure. The  $^{108}\text{Te}$  activity resulted from the proton decay of  $^{109}\text{I}$  which was below the detector threshold. Energies were computed using the single fit algorithm described in Section 5.1.

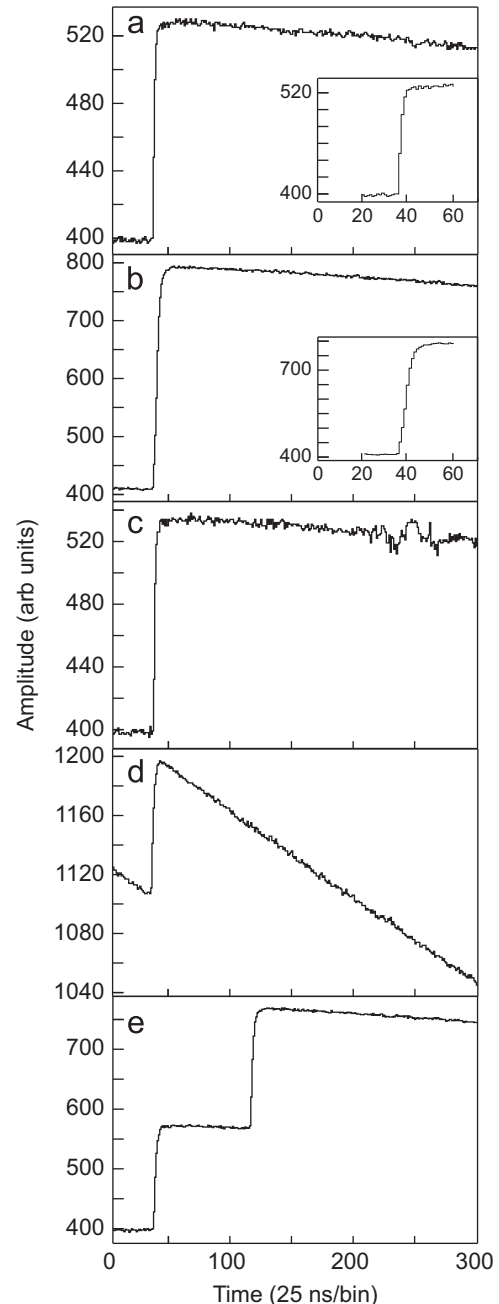


**Fig. 2.** Five characteristic traces displayed between 0 and 7.5  $\mu\text{s}$ . All pulses start at 1  $\mu\text{s}$ . (a) A normal single alpha decay pulse, (b) a slow rise time pulse, (c) a noisy pulse, (d) a pulse which occurred after a recoil before the preamplifier returned to baseline, (e) a pile-up pulse of two alpha decays. The insets in (a) and (b) expand the trace between 500 and 1.5  $\mu\text{s}$  to show the significant difference in rise time between the two pulses.

each strip  $\sim 1500$  individual traces were collected. However, for clarity the results from only one strip of the DSSD will be presented and discussed here, though the conclusions reached apply to the entire detector. The superpulse for each DSSD strip was created by averaging together acceptable traces. Unacceptable signals were eliminated from this averaging procedure if they had a slow rise time (see Fig. 2b), a non-monotonically decreasing tail, a sloping baseline (Fig. 2d), or an inappropriate energy range. Less than 1% of the source data set was removed by these conditions. The conditions also served to indirectly time-align the experimental signals for the superpulse averaging.

If too few pulses were averaged together the resulting superpulse would be a poor representation of the response of the detector strip and preamplifier chain. However, there is a point at which the inclusion of additional pulses fails to improve the quality of the superpulse due to the characteristic noise of the system. To determine this optimum number, nine separate superpulses were created by averaging a varying number of individual pulses from 1 to 1500 and are shown in Fig. 3. The degree to which each superpulse represented the ideal response to a 5.485 MeV alpha particle was determined by fitting the superpulse to a large sample of individual traces and inspecting the resulting  $\chi^2$  distribution. The fits were performed using the Minit package as implemented in the ROOT analysis framework [23]. For simplicity  $\chi^2$  will refer to the  $\chi^2$  per degree of freedom throughout this paper. The  $\chi^2$  distributions of the superpulses shown in Fig. 4. As might be expected, there is remarkable improvement in the  $\chi^2$  distributions going from a superpulse derived from 1 to 50 individual traces. However, there is no observable improvement averaging more than 50 traces. Therefore the minimum acceptable number of pulses for the creation of a superpulse was set at 50. The normalization of the resulting superpulse was chosen so that the superpulse amplitude was within a factor of ten from the experimental amplitude.

The above discussion has so far focused exclusively on the creation of a superpulse by averaging signals from an external alpha source. It was also possible to construct a superpulse based

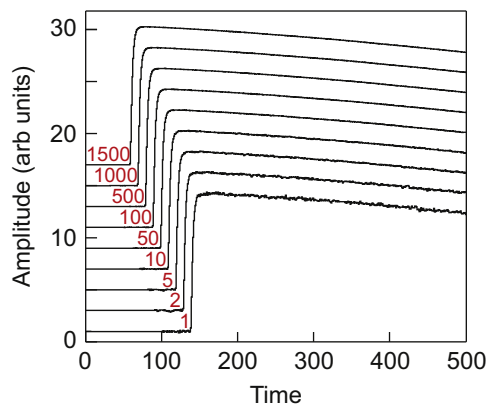


**Fig. 3.** The superpulses obtained by averaging a certain number (1, 2, 5, 10, 50, 100, 500, 1000, 1500) of individual pulses for one strip of the DSSD. There is qualitatively little difference between the superpulse derived with greater than 50 individual pulses. There is an artificial offset in both the vertical and the horizontal dimensions so that all superpulses are visible.

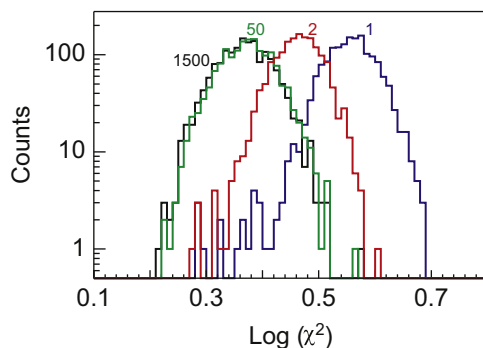


**Fig. 4.** The  $\chi^2$  distribution obtained by fitting the superpulses constructed from 1, 2, 50 and 1500 individual traces (shown in Fig. 3) to > 1500 individual pulses in one strip of the DSSD. There is a dramatic improvement in quality of the superpulse going from 1 to 50 traces evidenced by both a slight narrowing of the chi-square distribution and a large decrease in the centroid.

on the alpha decay of deposited  $^{109}\text{Te}$  activity during the experimental run. In this experiment, there was no appreciable difference in the quality of the superpulse constructed with greater than 50 experimental traces from either internal or external alpha decays. Additionally, there was no dependence of superpulse quality on the energy of the alpha particle used to create it (5.485 MeV or 3.107 MeV for the alpha decays from  $^{241}\text{Am}$  or  $^{109}\text{Te}$ , respectively). The energy dependence for superpulses created with less than 50 experimental traces was not investigated. In longer duration runs with higher implantation rates it was necessary to use the internal alpha decay from  $^{109}\text{Te}$  to create a superpulse which corrected for radiation damage induced changes to the pulse shape [14].

#### 4. Pulse shape analysis

The PSA of pile-up events was broken into two distinct stages:

- Stage 1: The identification of all traces that deviated from the ideal single-alpha pulse shape.
- Stage 2: Inspecting all of the non-ideal pulses for the presence of a pile-up signal due to two sequential alpha decays and, if present, extracting energy and time information.

The PSA was separated into two stages due to the unfortunate inability of algorithm used in stage 2 (described in Section 6) to differentiate between a pile-up pulse and a pulse due to the interaction of a single alpha particle with the Si detector introducing an unacceptable background of “false” pile-up pulses into the analysis. Further, the algorithm used in stage 2 is computationally intense with 4 independent parameters and takes considerably longer to perform than the two stage approach detailed here. Thus, the first stage of the analysis must eliminate as many of the single traces as possible while simultaneously retaining all pile-up pulses.

#### 5. Stage 1: pile-up pulse identification

In the first stage of the PSA each experimental trace was classified based on its deviation from the ideal pulse shape generated in Section 3 using three different methods:

- Single fit: fitting the superpulse to the experimental pulse.
- Derivative fit: fitting a derivative of the superpulse to a derivative of the experimental pulse.
- Time-over-threshold: summing the number of channels in the derivative trace that exceeded a certain threshold.

In each of the three methods a hard cut-off value was chosen which attempted to clearly differentiate those signals arising from the interaction of a single alpha decay in the DSSD and all other signals (those represented in Fig. 2b–e).

In order to investigate the performance of the three methods for selectively rejecting single alpha decay events, each one was applied to individual traces obtained under experimental conditions. The pulse amplitudes ranged between 1–6 MeV and include the alpha activities  $^{109}\text{Te}$ , and  $^{108}\text{Te}$ . The proton activity from  $^{109}\text{I}$  leading to  $^{108}\text{Te}$  was below the hardware threshold. The pile-up pulses of interest resulted from the sequential decay of  $^{109}\text{Xe}$  and  $^{105}\text{Te}$  due to the short half-life (620 ns [12]) of the latter. The total implantation rate was low enough that random pile-up signals were negligible. Beta decay signals were not observed due to the thickness of the detector (65  $\mu\text{m}$ ). The application of the three

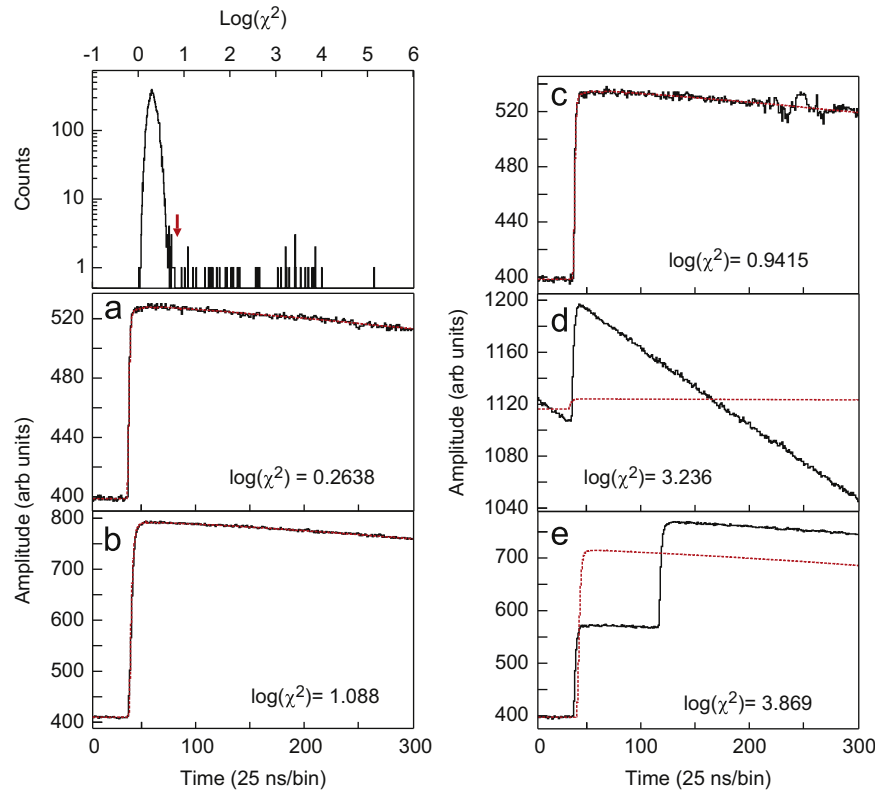


**Fig. 5.** The  $\chi^2$  distribution resulting from the fitting of a superpulse to the individual traces. The upper limit to be considered a single alpha trace was placed at 6.8 and is indicated by the red arrow. (a–e) The black solid lines are the same pulses as in Fig. 2a–e. The result of fitting the superpulse to the individual trace is shown by the red dashed line. For each fit the value of  $\log(\chi^2)$  is given. (For interpretation of the references to color in this figure legend, the reader is referred to the web version of this article.)

methods for characterizing the pulse shape is described in detail below.

### 5.1. Single-pulse fit method

For all recorded events the superpulse was fitted to the experimental trace using the MINUIT package provided in the ROOT analysis framework between a range of 250 ns and 7.5  $\mu$ s. Three parameters were included in fit; the pulse energy, the phase difference between the rise of the superpulse and the rise of the experimental pulse, and the baseline. The baseline of the pulse, determined by averaging the trace between 250 and 750 ns, was held fixed in the fit, leaving only two free parameters. Values of the superpulse between individual channels were obtained by linear interpolation to allow for the matching of the superpulse to the experimental trace with a time resolution finer than 25 ns (the intrinsic bin width due to the 40 MSPS of the digital electronics). The resulting  $\chi^2$  distribution is shown in Fig. 5. Also shown in Fig. 5 are the results of the single fitting procedure when applied to the sample signals presented in Fig. 2. The vast majority of analyzed signals have  $\chi^2$  values below 6.8 indicated by the arrow in the  $\chi^2$  distribution shown in Fig. 5. With this selection of  $\chi^2$  it was possible to efficiently discriminate between a normal pulse due to the emission of an alpha particle and all other signals shown in Fig. 2b–e.

### 5.2. Derivative fit method

The derivative method focuses on the rate of change of the trace amplitude and was attempted in an effort to accentuate the signature of a pile-up pulse as can be seen in Fig. 6e. Unfortunately, the pulses needed to be binned by a factor of two to reduce the influence of signal noise on the fitting procedure.

Similar to the single pulse fitting procedure the signal was fitted between the range of 250 ns and 7.5  $\mu$ s. Again, the only parameters in the fitting procedure were the height of the pulse, the phase difference, and baseline. The baseline was fixed by averaging the trace between 250 ns and 750 ns. The resulting  $\chi^2$  distribution is presented in Fig. 6. The traces shown in Fig. 6b–e are still separated from other signals enabling the determination of a single cut-off value of 8.5. However, the total range of  $\chi^2$  values is significantly reduced decreasing the separation between single and pile-up alpha decay events compared to the single fitting procedure.

### 5.3. Time-over-threshold method

Lastly, the total number of channels in the derivative trace above a certain threshold was used to differentiate between pulse shapes. The threshold which provided the greatest separation between single alpha and pile-up alpha decay events was empirically determined to be 10% of the maximum signal height in the derivative trace. The distribution of these time-over-threshold values is shown in Fig. 7 as well as the values for the five individual pulses from Fig. 2. The time-over-threshold technique while the least computationally intensive does not appear to give an adequate separation between the various pulse shapes of interest.

### 5.4. Stage 1 algorithm sensitivity

The effectiveness of the three different algorithms presented for distinguishing between a single alpha pulse and all other pulses can be based on two criteria:

- (1) the percentage of single traces which are not identified as such and

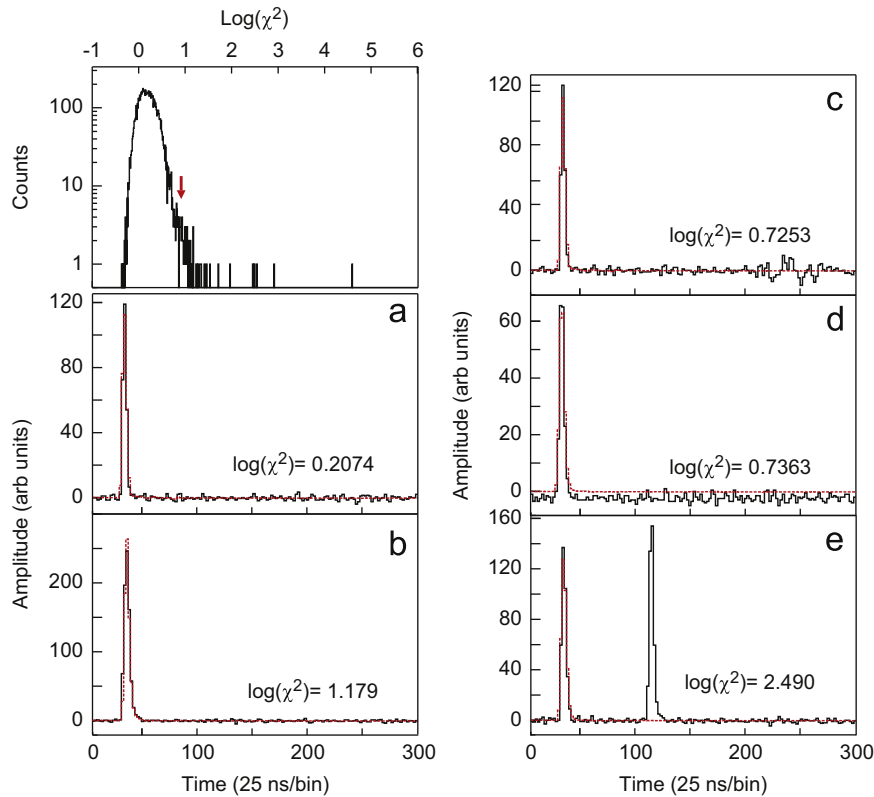


**Fig. 6.** The  $\chi^2$  distribution resulting from the fitting of the derivative of a superpulse to the derivative of an individual trace. The upper limit to be considered a single alpha trace was placed at 8.5 and is indicated by the red arrow. (a–e) The black solid lines are the same pulses as in Fig. 2. The result of fitting the derivative of the superpulse to the derivative of the individual trace is shown by the red dashed line. For each fit the value of  $\chi^2$  is given. (For interpretation of the references to color in this figure legend, the reader is referred to the web version of this article.)

(2) the percentage of double pulses which are falsely identified as single pulses.

If the percentage of (1) increases a larger background for the pile-up pulse is created whereas if the percentage of (2) increases the total number of identified pile-up pulses is decreases. The increase in either (1) or (2) negatively affects the pulse-shape processing routine. The performance of the three algorithms with respect to the first criteria can be observed by counting the number of traces above the hard cut off values in Figs. 5–7. In the data set presented here all three algorithms have a low percentage of misidentifying a single trace, with the single fit algorithm giving a slightly better performance than the derivative or time-over-threshold methods.

The algorithms performance with respect to the second criterion is critical as it determines, among other things, the minimum time separation between two pulses required for a pile-up trace to be successfully identified. The minimum time separation between the first and second pulse required for successful identification as a pile-up pulse should ideally be less than the half-life of the activity that produces the second pulse to maximize the total number of observable events. It is difficult to identify the minimum time separation based on the available experimental data since the event of interest, a pile-up of two alpha decays, is rare. Therefore, the response of the three algorithms to ideal pile-up pulses was explored. From the data already presented, experimental pulses which were well fit by a single superpulse (events with  $\log(\chi^2)$  values below 3.4 in Fig. 5) were selected and used to artificially construct a pile-up pulse by summing two copies of the single pulse as demonstrated in Fig. 8. This procedure allowed for the study of many pile-up pulses which are as close as possible to the experimental ones while also

allowing for the creation of pile-up pulses with both arbitrary relative amplitudes and time separations between the two alpha signals. Additionally, since pile-up pulses were created using experimental signals a broad range of total energies were sampled and detector noise was taken into account. In total, more than 8000 pile-up pulses were created, and this data set was used to determine the efficiency that the double pulse was identified as not originating from a single alpha decay for all three algorithms. Based on the algorithms discussed in Section 4 and their respective one-dimensional cutoffs (either a limit in  $\chi^2$  for the single or derivative fitting or a number of channels for time-over threshold) an ideal response to the simulated pile-up pulses would be a 100% identification of the pulses as not originating from a single alpha decay (thus a 0% loss of pile-up pulses, satisfying criterion (2)). The efficiency as a function of the time difference between the two alpha signals is shown in Fig. 9 for the three algorithms.

The single fit algorithm is the most robust identification method, clearly identifying 100% of pile-up pulses as not originating from a single alpha decay down to a time separation of 100 ns. Below this time difference it is increasingly difficult to differentiate a pile-up pulse from a single alpha decay. The derivative and time-over-threshold methods fare slightly worse, dropping in efficiency below 150 ns. This limit in time difference is a significant improvement over the older time threshold limit ( $\sim 500$  ns) used in previous studies [12,13]. Baring improvements to the acquisition hardware or further development in the PSA it will not be possible to identify a pile-up pulse with a time separation of  $\leq 4$  channels (25 ns/channel).

A similar investigation was also performed into the performance of the three algorithms as a function of the relative amplitude between the two alpha decay signals. The time

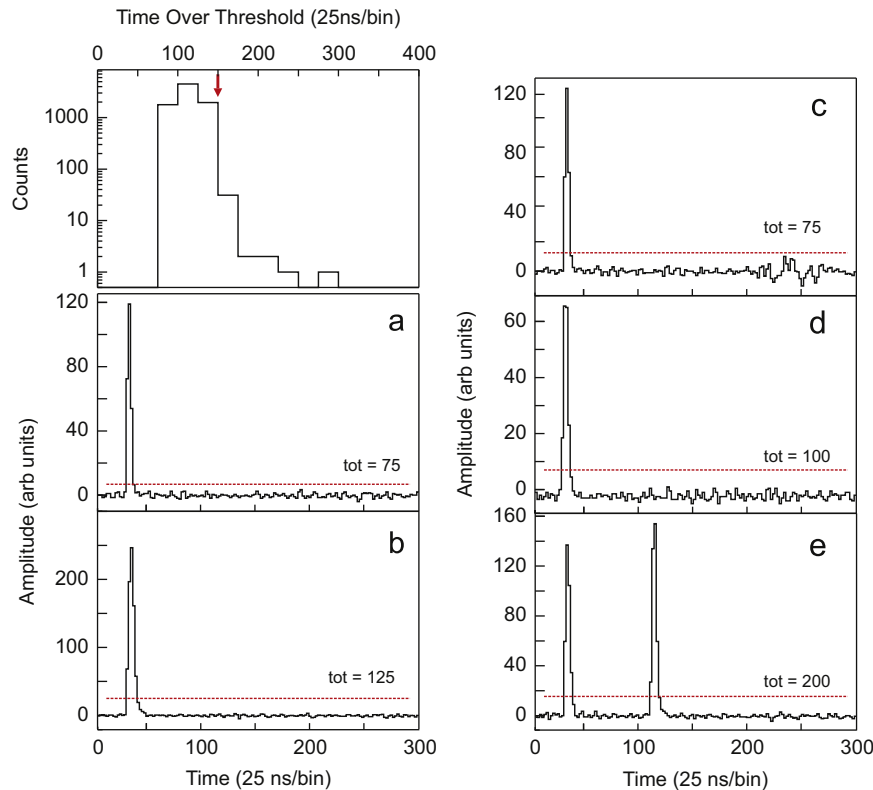


**Fig. 7.** The time-over-threshold distribution for a threshold set at 10% of the maximum in the derivative trace. The upper limit to be considered a single alpha trace was placed at 6 channels (150 ns) and is indicated by the red arrow. (a–e) The black solid lines are the same pulses as in Fig. 2. The red dashed line is placed at 10% of the maximum value of the derivative trace. The total time over this threshold is given.

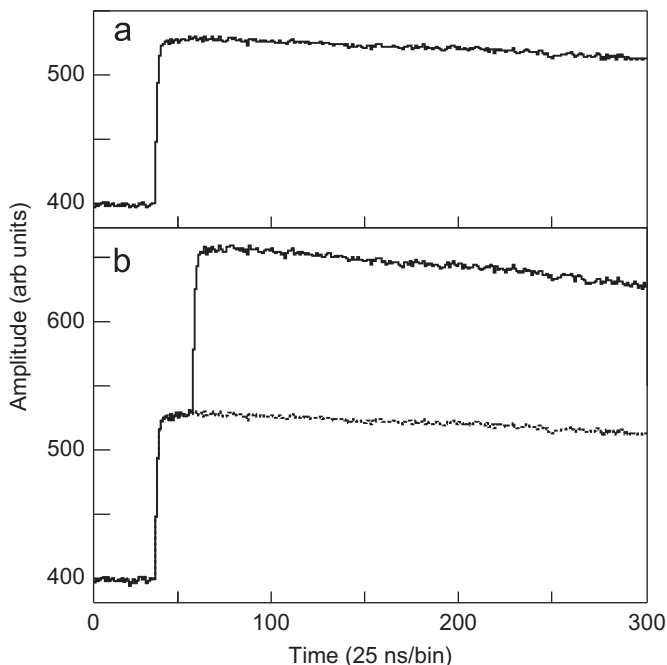


**Fig. 8.** Artificial pile-up pulse was constructed from experimental signals. (a) A typical experimental trace used to create an artificial pile-up pulse. (b) The pile-up pulse constructed from the trace in (a) with a 1:1 relative amplitude between the two traces and a time difference of 500 ns.

difference between the two alpha signal for this study was chosen to be 250 ns by which time all three methods have obtained their maximum efficiencies. The results are presented in Fig. 10. For

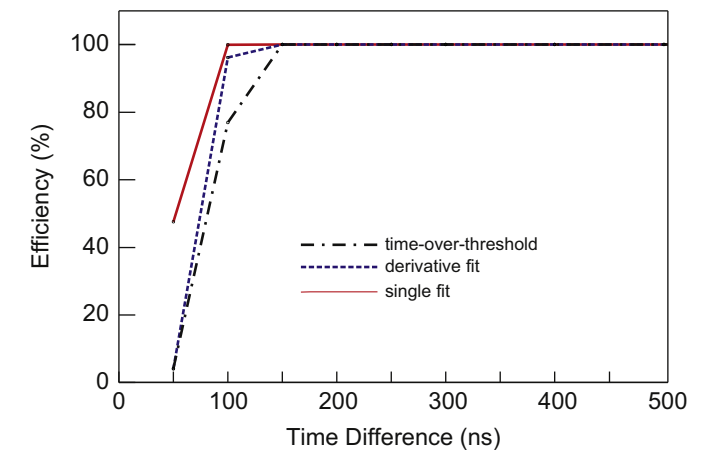


**Fig. 9.** The efficiency for identifying an artificially created pile-up alpha pulse as not originating from a single alpha interaction as a function of the time difference between the two pulses. The artificial pile-up pulse was constructed with equal energies for the first and second pulse. The total pulse amplitude ranged between 2 and 10 MeV. Three different detection methods are shown (red, solid) single fitting, (blue, dash) derivative fitting, and (black, dot-dash) time-over-threshold. See text for details. (For interpretation of the references to color in this figure legend, the reader is referred to the web version of this article.)

both single fitting and time-over-threshold, pile-up pulses can be identified with as much as a factor of 5 difference between their amplitudes which is important for the analysis of the pile-up pulses in which one of the alpha particles has escaped from the DSSD. It may be possible to improve the performance to lower time separations and/or greater relative amplitudes if a multi-parameter cut is used but such an investigation was not performed.

## 6. Stage 2: pile-up pulse characterization

The single fitting algorithm was selected as the first stage of the PSA for identifying all pulses which deviated from an ideal single alpha interaction with a Si detector. Starting with these signals, the second stage of the PSA involved the characterization of the pile-up pulses. To identify a pile-up pulse, the trace was fit

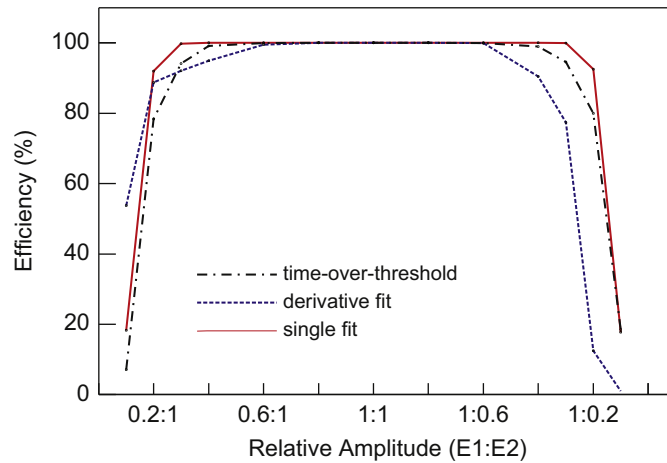


**Fig. 10.** The efficiency for identifying an artificially created pile-up alpha pulse as not originating from a single alpha decay as a function of the relative amplitude between the two pulses. The time difference was fixed at 250 ns. Three different detection methods are shown (red, solid) single fitting, (blue, dash) derivative fitting, and (black, dot-dash) time-over-threshold. See text for details. (For interpretation of the references to color in this figure legend, the reader is referred to the web version of this article.)

with the sum of two superpulses between 250 ns and 7.5  $\mu$ s. The baseline was determined from an average of the signal between 250 ns and 750 ns and was held fixed in the fit. The only adjustable parameters were the energies of the two superpulses and the time difference between them. The value of  $\chi^2$  was again used to determine the quality of the double superpulse fit and the distribution is shown in Fig. 11 for those events which were identified as not arising from an ideal single alpha interaction based on the single fitting method (Section 5.1 and Fig. 5). The superpulse pile-up fits and respective  $\chi^2$  values for the signals shown in Fig. 2a–e are presented in Fig. 11a–e. Traces with a  $\chi^2$  value below 8.5 were assumed to have been successfully fit as a pile-up pulse.

From Fig. 11a–e some qualitative comments on the pile-up fitting procedure can be advanced. First, the method efficiently picks out all pile-up pulses. Pulses with a sloping baseline can be rejected on the basis of their high  $\chi^2$  or, failing that, on the fact that the energy of the second extracted superpulse will be negative. However, the slow rise time and noise pulse (Fig. 11b, c) are more difficult to deal with. Though the  $\chi^2$  value for the noise pulse eliminates it from being considered a good pile-up event, a small change in its pulse shape would alter the situation. These two classes of pulses form the major background source for this particular identification scheme. Fortunately, while the rate of these background events is roughly comparable to the rate of true pile-up events they can be eliminated based on either extracted energy or timing information. In both the slow rise time and the noise trace presented in Fig. 11 the extracted time difference between the first and second superpulse is less than 100 ns. This value marks an additional limit for this PSA independent of the ability to effectively identify pile-up pulses presented in Section 5.

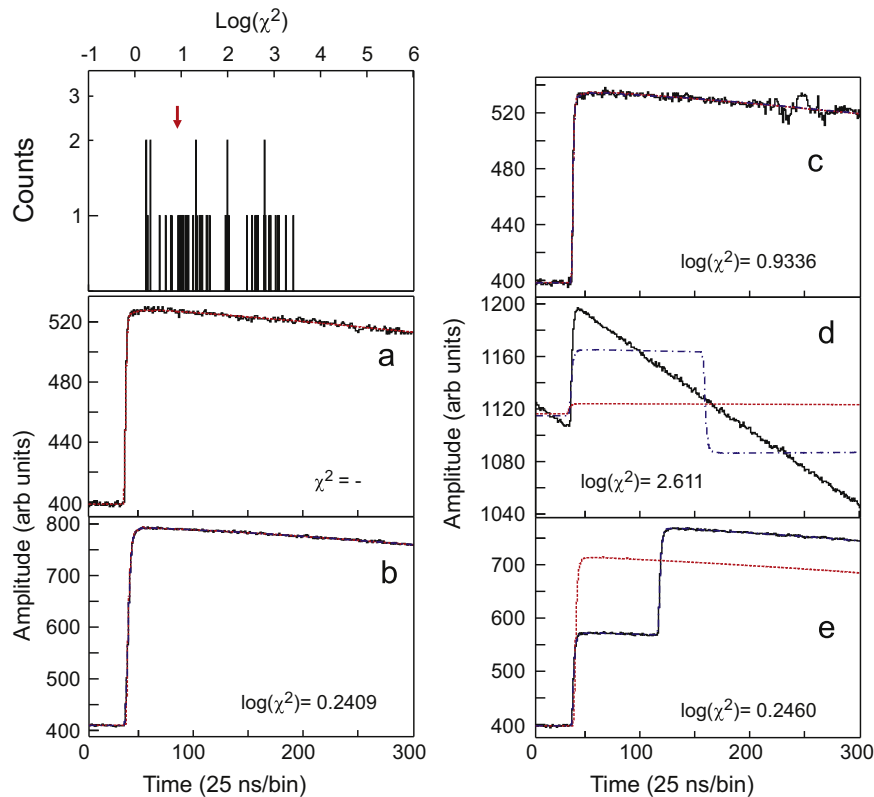


**Fig. 11.** The  $\chi^2$  distribution resulting from the fitting of selected experimental traces which were not well described by a single alpha decay with a pile-up superpulse (i.e. those signals above the red arrow in Fig. 5), see text for details. (a–e) The black solid lines are the same pulses as in Fig. 2. The red dashed line is the result of the single superpulse fit. The blue dot-dash line is the result of the pile-up superpulse fit. The trace presented in (a) was identified as a single and thus no double superpulse fit was attempted. (For interpretation of the references to color in this figure legend, the reader is referred to the web version of this article.)

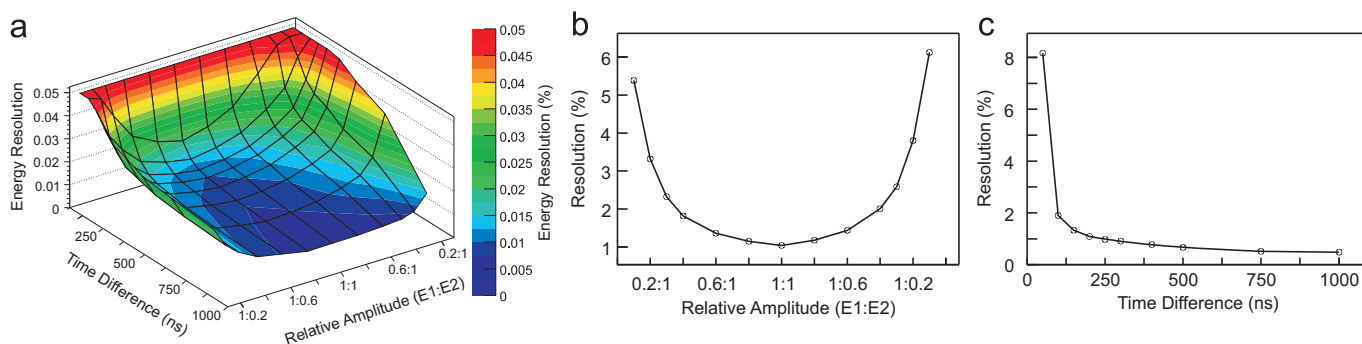


**Fig. 12.** (a) The energy resolution of the pile-up pulse characterization algorithm in percent as a function of the relative amplitude and time difference in nanoseconds between two alpha decay pulses. (b) The energy resolution as a function of relative amplitude for a time difference of 250 ns. (c) The energy resolution as a function of time difference for a 1:1 relative amplitude.

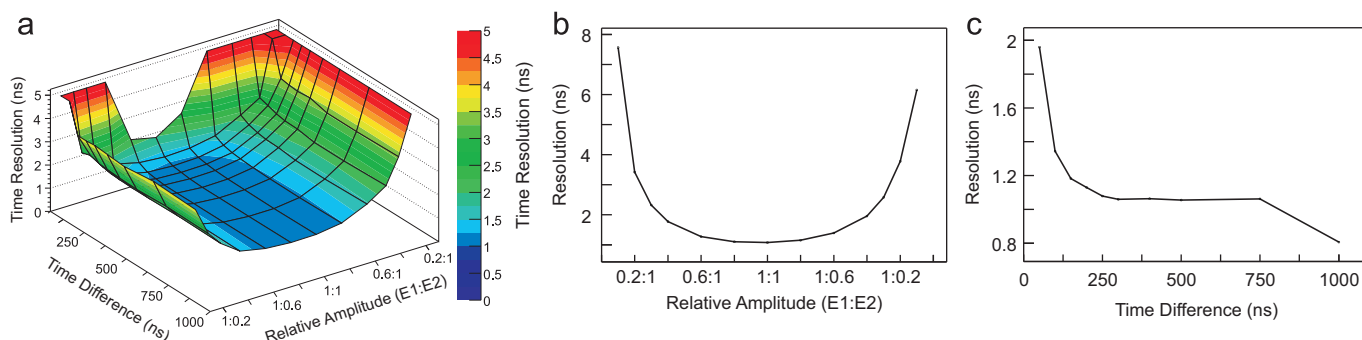


**Fig. 13.** (a) The time resolution of the pile-up pulse characterization algorithm in nanoseconds as a function of the relative amplitude and time difference between two alpha decay pulses. (b) The time resolution as a function of relative amplitude for a time difference of 250 ns. (c) The time resolution as a function of time difference for a 1:1 relative amplitude.

### 6.1. Sensitivity limits

A spectroscopic measurement of the two distinct alpha decays in the chain  $^{109}\text{Xe} \rightarrow ^{105}\text{Te} \rightarrow ^{101}\text{Sn}$  requires both the identification of the pile-up pulse described previously but also a precise measurement of the amplitudes of both alpha decay pulses and the time separation between them. The obtainable energy resolution of the algorithm depends on a multitude of factors including, but not limited to; preamplifier noise, the number of bits used in the ADC, the energy of the two alpha decays and their relative amplitudes of their respective pulses, and the time difference between the two alpha decays. The same procedure described in Section 5.4 to compare the stage 1 algorithms is used here as well to extract the energy and time resolution of the pile-up characterization algorithm since the amplitude and time differences used to construct the artificial pile-up pulse are known a priori. The energy resolution as a function of relative amplitude and time between two pulses is shown in Fig. 12a. A representative one-dimensional slice through Fig. 12a showing the obtainable energy resolution as a function of relative amplitude with a fixed time difference of 250 ns is shown in Fig. 12b. The rapid degradation of energy resolution as a function of relative amplitude arises mainly from the small number of ADC bits used to record the alpha decay [16] with a smaller additional contribution from preamplifier noise. The energy resolution as a function of time difference is shown in Fig. 12c at a 1:1 relative amplitude. The curve is qualitatively similar to that obtained in Ref. [24] but with a lower achievable time difference. The time difference at which the energy resolution begins to dramatically rise is located at around 100 ns. It should be kept in mind that with the hardware used in the present study a 100 ns time difference corresponds to only four channels separating the two alpha decay pulses and is

consistent with the minimum time separation required for identification derived earlier. The easiest method to improve the time resolution indicated in Fig. 12c is to increase the sampling speed of the digitizers. If the digitizers were able to sample the incoming signal at 100 MSPS instead of the 40 MSPS used in this study then the minimum time separation between signals would be reduced to 40 ns. The time resolution as a function of both relative amplitude and time different is shown in Fig. 13.

## 7. Summary

In summary, a two stage PSA has been developed for the selective identification and characterization of a pile-up pulse resulting from two successive alpha decays in a Si detector. The first stage consisted of rejecting all events that could be described as a single alpha decay and was performed with three different algorithms (single fitting, derivative fitting, and time-over-threshold) with the single fitting method providing the best performance. This stage is limited to a time separation between the two alpha particles of 100 ns. Below this value the pile-up pulses become buried in a larger background of slow rise time and noisy traces. The derivative method is also promising but suffers in our specific application due to the need to bin the experimental signal due to the noise on the Si detector. Using the selected subset of events the second stage was a fit of two superpulses to the experimental trace, varying the amplitudes and time separation. While only alpha signals in a silicon detector are discussed the techniques should be applicable to any signal with the characteristic shape described herein. The algorithm presented here promises to be extraordinary useful in cases where energy pulses from distinct decay events pile-up such as further sequential

alpha decay studies on  $^{108}\text{Xe}$ , superheavy element research, and microsecond isomeric activity.

### Acknowledgments

This work was supported in part under US DOE Grants DE-FG02-96ER40983 (UT), the NNSA under the Stewardship Science Academic Alliances program through DOE Cooperative Agreement No. DE-FG52-08NA28552, and the National Science Foundation under Grant no. PHY-0606007.

### References

- [1] R.J. Cooper, et al., Nuclear Instruments and Methods in Physics Research Section A 629 (2011) 303.
- [2] I. Abt, et al., Nuclear Instruments and Methods in Physics Research Section A 577 (2007) 574.
- [3] M. Descovich, et al., Nuclear Instruments and Methods in Physics Research Section A 553 (2005) 535.
- [4] P.-A. Soderstrom, et al., Nuclear Instruments and Methods in Physics Research Section A 638 (2011) 96.
- [5] R.J. Cooper, et al., Nuclear Instruments and Methods in Physics Research Section A 579 (2007) 313.
- [6] M. Schwenke, et al., Nuclear Instruments and Methods in Physics Research Section A 650 (2011) 73.
- [7] L. Bardelli, et al., Nuclear Instruments and Methods in Physics Research Section A 521 (2004) 480.
- [8] M. Madurga, et al., AIP Conference Proceedings 1336 (2010) 586.
- [9] S. Yousefi, et al., Nuclear Instruments and Methods in Physics Research Section A 598 (2009) 551.
- [10] R. Grzywacz, et al., Nuclear Instruments and Methods in Physics Research Section A 261 (2007) 1103.
- [11] L. Bardelli, et al., Nuclear Instruments and Methods in Physics Research Section A 23 (2011) 20. doi:10.1016/j.nima.2011.06.063.
- [12] S.N. Liddick, et al., Physical Review Letters 97 (2006) 082501.
- [13] S.N. Liddick, et al., European Physical Journal Special Topics 150 (2007) 131.
- [14] I.G. Darby, et al., Physical Review Letters 105 (2010) 162502.
- [15] K. Rykaczewski, et al., Nuclear Physics A 682 (2001) 270c.
- [16] M. Karny, et al., Physical Review Letters 90 (2003) 012502.
- [17] R. Grzywacz, et al., European Physical Journal A 25 (s01) (2005) 145.
- [18] A.P. Robinson, et al., Physical Review C 68 (2003) 054301.
- [19] J.C. Batchelder, et al., Physical Review C 57 (1998) R1042.
- [20] D.T. Joss, et al., Physical Letters B 28 (2006) 34.
- [21] C.J. Gross, et al., Nuclear Instruments and Methods in Physics Research Section A 450 (2000) 12.
- [22] R. Grzywacz, Nuclear Instruments and Methods in Physics Research Section B 204 (2003) 649.
- [23] R. Brun, F. Rademakers, Nuclear Instruments and Methods in Physics Research Section A, 389 (1997) 81. See also <<http://root.cern.ch/>>.
- [24] M. Nakhostin, et al., Review of Science Instruments 81 (2010) 103507.